Anomalously thin transition zone and apparently isotropic upper mantle beneath Bermuda: Evidence for upwelling

Margaret H. Benoit
Department of Physics, College of New Jersey, Ewing, New Jersey, USA (benoit@tcnj.edu)

Maureen D. Long
Department of Geology and Geophysics, Yale University, New Haven, Connecticut, USA

Scott D. King
Department of Geosciences, Virginia Tech, Blacksburg, Virginia, USA

[1] The origin of the Bermuda swell and volcanism remains enigmatic. The lack of an associated time-progressive hotspot track and absence of present-day volcanic activity make it difficult to reconcile with a deep mantle plume model. We analyze shear wave splitting measurements to estimate mantle flow direction and receiver function stacks to place constraints on the mantle transition zone thermal structure. *KS phases exhibit well-resolved null arrivals (no splitting) beneath the swell over a range of back azimuths. We find that the 410 and 660 km discontinuities are 49 ± 5 km and 19 ± 5 km deeper than the global average, respectively, leading to a transition zone thickness that is 27 ± 4 km thinner than the average. Together, an apparently isotropic upper mantle and a thinned mantle transition zone suggest that mantle flow is primarily vertical beneath the swell, consistent with the presence of hot, buoyant mantle at depth.

1. Introduction

[2] Bermuda rise is a 1500 km, NE-SW-trending, oval-shaped, basement rise that lies 600–800 km ESE of the Eastern North American Margin (Figure 1), sitting atop 100–140 Ma ocean crust [cf. *Vogt and Jung*, 2007]. Uplift was initiated in the Middle Eocene (~48–45 Ma), and appears to have continued through the Middle Oligocene, though the onset of volcanism is not well constrained [*The Shipboard Scientific Party*, 1979; *Tucholke and Vogt*, 1979; *Vogt and Jung*, 2007]. While Bermuda is included in many hotspot compilations [e.g., *Davies*, 1988; *Sleep*, 1990], it is difficult to define a time-progressive hotspot track or plume head associated with Bermuda [*Morgan*
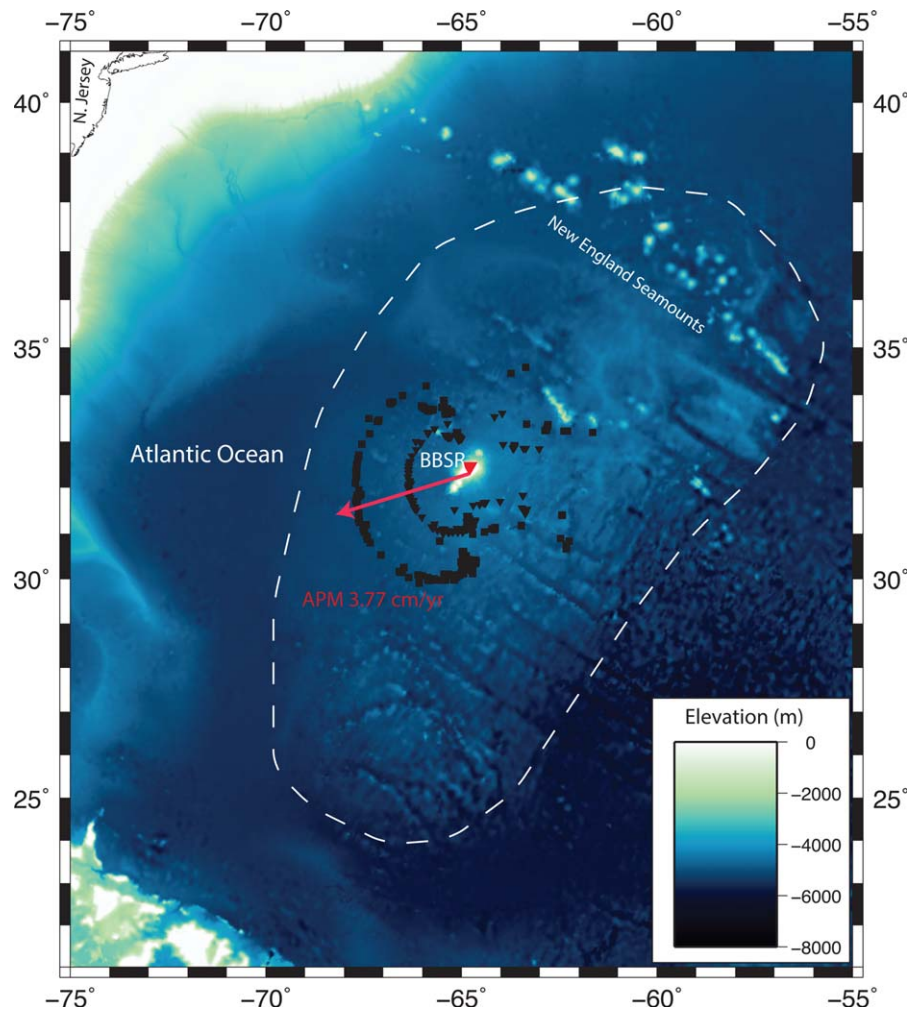
Figure 1. Map of Bermuda swell, outlined by dashed white line, showing the location of station BBSR and P410s (black triangles) and P660s (black squares) pierce points. The red vector shows the absolute plate motion (APM) of *Gripp and Gordon* [2002].

and Crough, 1979]. At the predicted present day location of the hotspot, approximately 1000–1500 km northeast of the islands on the outer edge of the Bermuda rise, there is no anomalous volcanic activity, nor is there any volcanic activity southwest of Bermuda between the continental shelf and Bermuda rise [*Morgan*, 1983; *Duncan*, 1984; *Mueller et al.*, 1993; *Vogt and Jung*, 2007]. *Sleep* [2002] proposed that as the Bermuda plume approaches the mid-Atlantic ridge the buoyant, upwelling plume material deflects toward the ridge, forming a gap in the hotspot track. Yet along the relevant section of the mid-Atlantic ridge there is a local topographic low [e.g., *Vogt and Jung*, 2007], not a local topographic high as would be expected as the upwelling plume locally uplifts the ridge. Overall, Bermuda scores poorly on the criteria associated with a deep mantle plume origin for hotspot volcanism [e.g., *Courtillot et al.*, 2003; *Anderson*, 2005].

[3] Alternative models for the formation of Bermuda that do not invoke a deep mantle plume origin have also been explored. Based on the distance between the rise axis and the eastern North American continent/ocean boundary, the Bermuda rise is one of a number of hotspots that is geometrically favorable for edge-driven convection (EDC) [*King*, 2007]. Similarly, *King and Ritsema* [2000] point out that fast shear wave anomalies beneath the West African and South American cratons are consistent with the downwelling limbs of EDC cells [*King and Anderson*, 1998] and they hypothesize that a number of hotspots on the African and South American plates correspond to the upwelling limbs of the same EDC cells.

[4] *Vogt and Jung* [2007] explored the possibility that the location of Bermuda rise is controlled by pre-existing lithospheric structures. They point out that Bermuda rise occurs on crust that is rough (450–1200 m relief) and was created during a period of ultra-slow spreading (8 mm/a half-rate). *Lizarralde et al.* [2004] determined the seismic structure along a line across the southern Bermuda rise and found the crust is approximately 1.5 km thinner than the smoother (150–450 m relief) and rapidly formed (13–14 mm/a) crust to the west. *Vogt and Jung* [2007] point out that, however, that even if lithospheric control plays a role, it does not explain the source of the magma that formed Bermuda. The possibility of lithospheric control of the structure of Bermuda was also raised by *Crough* [1983], who suggested that the bathymetric swell is supported by lithospheric thinning and moves with the North American plate.

[5] Observations of transition zone structure and upper mantle anisotropy can serve as a test of both the mantle plume and edge-driven convection models for the origin of Bermuda, as they provide indicators of radial mantle structure and possible mantle flow geometries. While both a plume and the upwelling limb of an edge-driven convection cell would result in a thinner than the average transition zone, an elevated 660 km discontinuity would be more consistent with a deep mantle plume model. Predominantly vertical mantle flow would likely result in vertical preferential alignment of olivine fast axes; therefore, a vertical axis of anisotropic symmetry would be expected in the upper mantle for both scenarios. This would in turn manifest as very weak *KS splitting or predominantly null (no splitting) *KS arrivals. To assess the mantle structure beneath Bermuda, here we compile shear wave splitting measurements and receiver function stacks from permanent station BBSR, which has operated continuously since 2002.
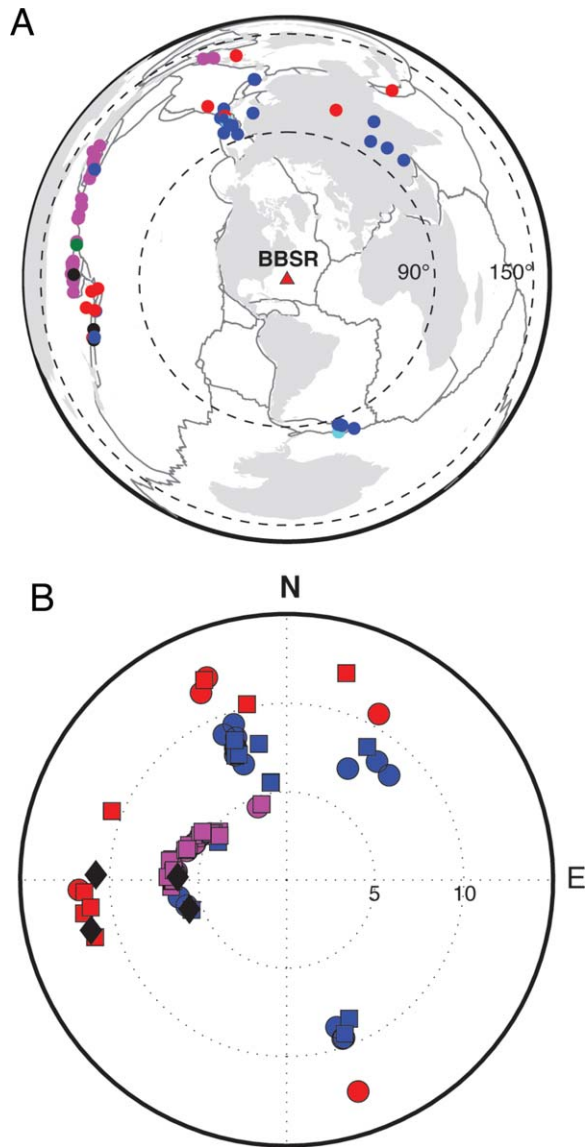
2. Shear Wave Splitting Analysis

[6] In order to constrain the geometry of upper mantle anisotropy beneath Bermuda, we analyzed the splitting of SKS, SKKS, and PKS waveforms recorded at BBSR during the period October 2008-February 2013, after the station had new hardware installed. Our measurement procedure, which closely follows our previous work [*Long et al.*, 2010], used the SplitLab software [*Wüstefeld et al.*, 2007] to carry out the rotation-correlation and transverse component minimization measurement meth-

ods simultaneously. Seismograms were bandpass filtered between 10 and 25 s before measurement. All measurements were assigned a quality factor (A, B, or C) based on signal-to-noise ratio (SNR) and linearity of the initial particle motion (for null arrivals) or on the error estimates and consistency between the measurement methods (for non-nulls).

[7] Our procedure yielded 88 total measurements (33 SKS, 18 SKKS, and 37 PKS) from 81 separate earthquakes in the 90°–150° epicentral distance range (Figure 2a). Of these 88 measurements (Figure 2b), 84 (95%) were null (that is, nonsplit) arrivals. Of these null arrivals, 68 were characterized as A or B quality and 29 were rated A. All of the non-null measurements were characterized as C quality, with relatively small delay times (0.6–0.8 s) and poorly resolved fast directions that ranged from −38° to −70°. The null measurements cover a range of backazimuths, with excellent coverage throughout the 255°–345° backazimuthal quadrant. All splitting measurements are listed in supporting information[1] Tables S1 and S2, and a set of high-quality null waveforms from a range of backazimuths is shown in Figure 3.

[9] These observations suggest that the upper mantle beneath station BBSR does not generally cause splitting of *KS waveforms at the periods examined in this study. In the context of this interpretation, the few non-null *KS measurements we identified may represent localized contributions from weak anisotropy in the shallow lithosphere [e.g., *Long et al.*, 2010] or in the deep mantle [e.g., *Lynner and Long*, 2012]. Alternatively, given the very large error bars on the non-null measurements in our data set, each of which is quality C (supporting information Table S1), an equally plausible explanation is that these measurements actually represent spurious transverse component noise that is being misinterpreted by the shear wave splitting algorithm, rather than true *KS splitting. In either case, the non-null measurements we report are highly unlikely to correspond to well-constrained anisotropy in the upper mantle directly beneath the station. A recent global model of upper mantle azimuthal anisotropy derived from surface waves [*Lebedev and van der Hilst*, 2008; *Becker et al.*, 2012] exhibits significant (∼2%) anisotropy beneath the North Atlantic, with a WNW-ESE fast direction. Therefore, it is plausible that the lack of splitting we observe

---

[1]Additional supporting information may be found in the online version of this article.

Figure 2. (a) Event locations for all events that yielded at least one usable shear wave splitting measurement. Colors indicate the type of phase used: SKS only (blue), SKKS only (red), PKS only (magenta), SKS/SKKS (cyan), and PKS/SKKS (green). Events that yielded at least one non-null splitting measurement are shown in black. BBSR station location is shown with a red triangle. Dashed lines indicate the 90° and 150° epicentral distance ranges. (b) Stereoplot of splitting results, plotted as a function of backazimuth and incidence angle. Null measurements are shown in color, with colors indicating phase type (blue for SKS, red for SKKS, and magenta for PKS). Circles indicate quality A measurements and squares indicate quality B measurements. Non-null measurements (all of quality C) are shown with black diamonds; fast directions, delay times, and interpretations of these measurements are discussed in the text.

beneath BBSR represents a localized perturbation to the larger scale anisotropic structure beneath the Atlantic basin.

[10] Because Bermuda is located in the middle of an ocean basin, the interpretation of *KS splitting (or lack thereof) beneath BBSR is likely free from many of the common complications, such as the presence of fossil lithospheric fabric (such as in continental settings) [*Fouch and Rondenay*, 2006], a contribution from aligned partial melt (such as in
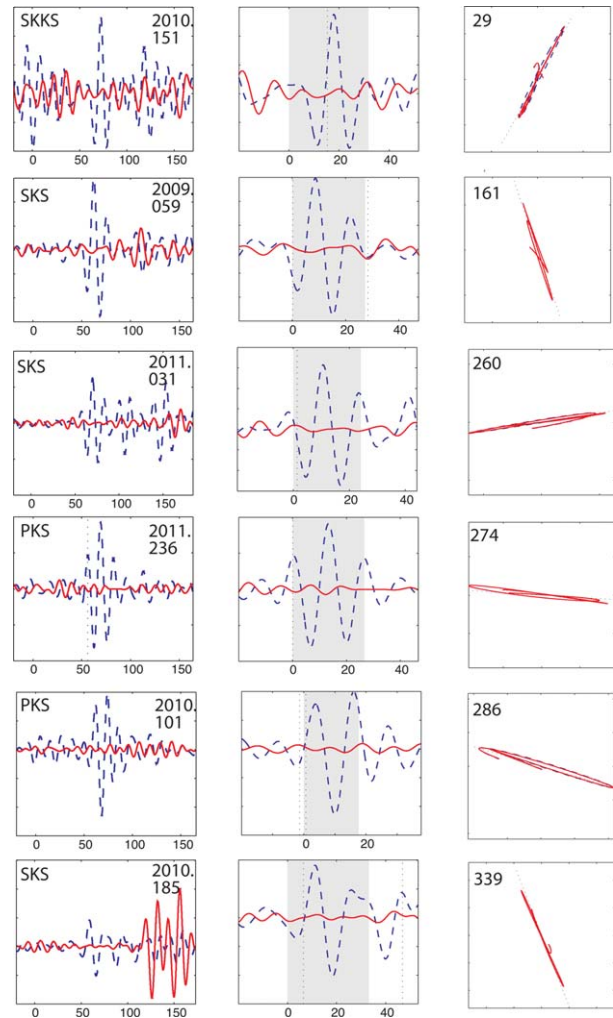
Figure 3. Examples of quality "A" null measurements from a range of backazimuths. (left) Radial (dashed blue line) and transverse (solid red line) components of uncorrected waveforms for a time window of approximately 160 s centered on the expected arrival time of the phase used in the analysis. Time in seconds is shown on the x axis; the phase type is shown in the top left, and the year and Julian day of the event is shown in the top right. In some cases, later phase arrivals can be observed (e.g., SKS_{df} and SKKS for event 2011.031; S_{diff} for event 2010.185) in the time windows shown. (middle) The same waveforms as the left, but a shorter time window is shown, and the gray box indicates the time window used to generate the particle motion plots. (right) The corresponding particle motion diagram for each waveform, with the event backazimuth shown in the top left.

extensional regimes) [e.g., *Blackman and Kendall*, 1997; *Barclay and Toomey*, 2003], or fabric transitions and/or complex flow (such as in subduction settings) [e.g., *Long*, 2013]. We suggest, therefore, that the most plausible interpretation of our observations is that the upper mantle beneath Bermuda exhibits a vertical axis of fast anisotropic symmetry, as might be expected for vertical mantle flow (i.e., upwelling). Alternative explanations for our observations do exist; predominantly null measurements can also indicate isotropic upper mantle, very complicated anisotropic structure that varies over short length scales (resulting in weak effective anisotropy), or two layers of anisotropy whose fast directions are offset by exactly $90°$, effectively canceling each other out. While we cannot completely rule out these possibilities, given the presence of anisotropy elsewhere in the Atlantic basin [*Becker et al.*, 2012; *Debayle and Ricard*, 2013] and the configuration of the fossil spreading direction and present-day plate motion, these scenarios seem less likely than our preferred interpretation of a vertical axis of anisotropic symmetry.

3. Receiver Function Analysis

[11] We examined P to S converted energy from the 410 km to 660 km mantle discontinuities beneath Bermuda using radial receiver functions. The 410 km discontinuity is usually interpreted as a mineral phase transformation from α-olivine to wadsleyite, and the 660 km discontinuity has been demonstrated to represent the olivine phase change from ringwoodite to perovskite and magnesiowustite (hereafter referred to as the "410" and "660," respectively) [e.g., *Ringwood*, 1983; *Jackson*, 1983]. Temperature variations in this region of the mantle will cause the mantle transition zone to thicken or thin because of the positive and negative Clapyron slopes for the 410 and 660, respectively [*Katsura and Ito*, 1989; *Bina and Helffrich*, 1994]. Hydration and compositional variations also play a significant role in determining the depth of these phase transformations [e.g., *Fei and Bertka*, 1999; *Smyth et al.*, 2006; *Smyth and Frost*, 2006; *Leahy and Bercovici*, 2007].

[12] Receiver functions were computed using the time-domain deconvolution method of *Ligorría and Ammon* [1999] with a Gaussian filter of 0.7 (similar to a low-pass filter of with a corner frequency of 0.35 Hz). We retained only receiver functions that fit at least 80% of the signal during deconvolution, and all receiver functions were visually inspected to remove any with excessive

harmonic oscillation or very large negative troughs after the initial P arrival. In total, 228 out of a possible 998 receiver functions met our selection criteria. The events were distributed over a large range of backazimuths, though most events arrived from the south and northwest. Figure 1 shows the distribution of pierce points for the Pds phases at 410 and 660 km depth.

[13] Receiver functions were moveout corrected and depth converted [*Kind and Vinnik*, 1988], and then stacked by summing the amplitudes of the receiver functions at 1 km intervals in depth. We applied the phase-weighting algorithm of *Schimmel and Paulssen* [1997] to remove spurious long period and incoherent noise from the stacks, and a weighting factor ν of 1 was used to produce the stacks presented in this study [*Frassetto et al.*, 2010, *Long et al.*, 2010].

[14] Figure 4 shows the station-averaged raw and phase-weighted stacks of mantle discontinuity structure that were depth corrected using (1) ak135 [*Kennett et al.*, 1995] with oceanic crustal correction and (2) a model based on the global tomography model R40RTS [*Ritsema et al.*, 2010]. In this second model, S velocities were ~1.5% faster than ak135 between 0 and 150 km depth and ~1% slower between 150 and 800 km depth; corresponding P-wave speeds were calculated using a 10% higher Vp/Vs ratio than that of ak135 between 150 and 800 km depth. We note that other global tomographic models show shear wave speeds that are very similar to those found in R40RTS for the region of interest (e.g., S362ANI [*Kustowski et al.*, 2008]; SAW642AN [*Panning and Romanowicz*, 2006]; TX2008 [*Simmons et al.*, 2009], and HMSL-S [*Houser et al.*, 2008]).

[15] There was little variation in the absolute depths of the 410 and 660 km discontinuities between the two different velocity models that we tested. We found an average depth for the 410 of 455 km and an average depth of 670 km for the 660, resulting in an average transition zone thickness of 215 km. This is significantly thinner than the global average of 242 km [*Gu et al.*, 1998, *Lawrence and Shearer*, 2006]. Stacks over a range of back azimuths do not conclusively show a systematic geographical variation in transition zone thickness, due to the fact that most of the events are clustered within two small backazimuthal zones to the south and west. No pulse corresponding to the 520 km discontinuity was observed, which is normally attributed to a relatively small impedance contrast caused by the wadsleyite to
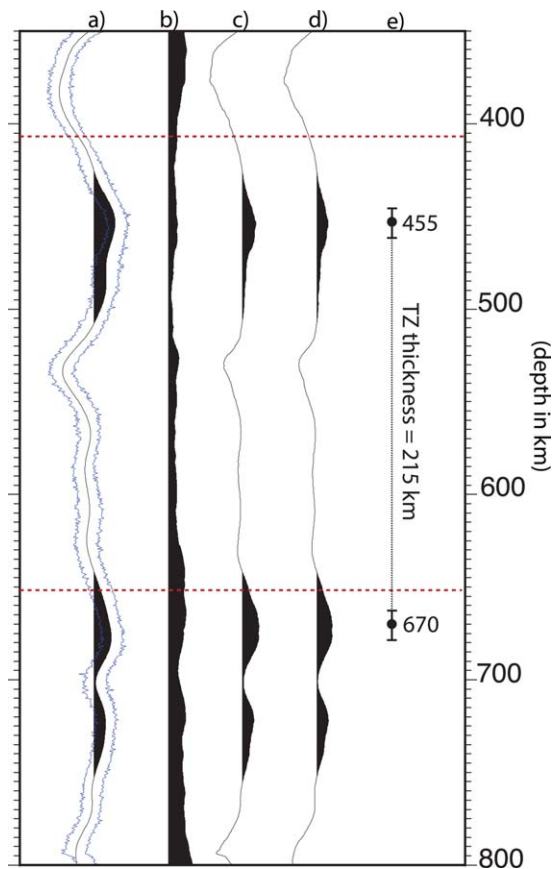
Figure 4. (a) Unweighted depth-migrated stack for station BBSR with 95% confidence interval bounds plotted as thin blue lines. (b) The phase-weight filter used to compute depth-migrated stacks using (c) ak135 [*Kennett et al.*, 1995] and (d) ack135 modified using R40RTS [*Ritsema et al.*, 2010]. (e) The depths of the transition zone discontinuities with error bars and the overall transition zone thickness along with the global average depths for the discontinuities from *Lawrence and Shearer* [2006] shown in red.

ringwoodite phase change at this depth [*Shearer*, 1990]. This phase is globally intermittent [e.g., *Flanagan and Shearer*, 1998; *Gu et al.*, 1998] and does not seem to be well correlated with mantle potential temperature, temperature variations, or water content [e.g., *Juliá and Nyblade*, 2013]. Emerging research suggests that the discontinuity may be related to variations in Fe, Mg, or Ca content, but these correlations are speculative at this point [e.g., *Saikia et al.*, 2008; *Juliá and Nyblade*, 2013]. A pulse with amplitude similar to that of the 410 was observed at 700 km depth, resulting in a "double" 660. Double 660 km discontinuities are generally attributed to the presence of ilmenite in the lower mantle [*Wang et al.*, 1994].

[16] Error estimates for the discontinuity depths shown in Figure 4e are based on several factors.

The absolute depths of the discontinuities are dependent on the velocity model used for the depth correction, but a significant deviation from this model, particularly with respect to the Vp/Vs ratio used would be a source of error. The seismic velocity structure of the central Atlantic Ocean is largely unconstrained, but realistic variations if the Vp/Vs ratio would cause the depth of the 410 and 660 to vary by as much as 3 km. Since global seismic tomography models suggest that most of the upper mantle and transition zone are relatively slow, it is likely that the Vp/Vs ratio in this region may be slightly elevated. If the mantle was hydrated in this region, Vp/Vs ratios would also be expected to be elevated [*Smyth and Frost*, 2006; *van der Lee and Wiens*, 2006]. If we assume that Vp/Vs ratios are 10% higher than ak135, the errors in the depth of the 410 km discontinuity would be at most 2 km and 2 km for the depth of the 660 km discontinuity, as shown in Figure 4.

[17] The effect of upper mantle anisotropy may also affect the relative timing of Ps-P phases. The shear wave splitting results from station BBSR suggest that the mantle is either isotropic or has a vertical axis of fast symmetry. In the case of an isotropic mantle, there would be error associated with the relative timing of the Ps-P phases. In the case of a vertical fast axis, a realistic model of a 2% anisotropy within a ~150 km thick layer would produce a timing error ~0.5 s, resulting in at most a 5 km error in absolute depths of the discontinuities, but this error would be almost negligible for the relative transition zone thickness.

[18] The overall transition zone thickness, as opposed to the absolutely depths of the individual discontinuities, is generally insensitive to crust and upper mantle velocity variations and anisotropy. Uncertainties in the velocity structure of the transition zone itself are the main source of uncertainty in our estimates of transition zone thickness. Assuming that transition zone shear velocities are ~0.75%–1.25% slow, similar to the shear velocities in several global seismic tomography models (e.g., R40RTS [*Ritsema et al.*, 2010], S362ANI [*Kustowski et al.*, 2008], SAW642AN [*Panning and Romanowicz*, 2006], TX2008 [*Simmons et al.*, 2009], and HMSL-S [*Houser et al.*, 2008]), maximum errors in the thickness of the transition zone would be less than 2 km. Also, the plane-wave approximation method that we used to make the time-to-depth conversion [*Kind and Vinnik*, 1988] tends to underestimate the travel time differences between Ps-P phases, that can result in an overestimation of the transition zone thickness of up to 4

km [*Lawrence and Shearer*, 2006]. Therefore, our transition zone thickness is likely overestimated slightly, though it is significantly thinner than the global average by ~27 km.

4. Discussion

[19] Our inferences of a significantly thinned transition zone and a radially isotropic upper mantle are most consistent with the presence of hot, buoyant upwelling mantle at depth beneath Bermuda. The observation of a depressed 660 km discontinuity suggests that the hot thermal anomaly does not extend down through the transition zone and is more easily reconciled with edge-driven convection than a mantle plume. However, this inference is inconsistent with the slow S velocity anomalies that extend through the transition zone into the lower mantle beneath Bermuda in several recent global tomographic models (including R40RTS [*Ritsema et al.*, 2010], S362ANI [*Kustowski et al.*, 2008], and SAW642AN [*Panning and Romanowicz*, 2006]).

[20] We estimate the temperature anomaly in the transition zone using the formulation of *Helffrich* [2000] and substituting in the global average transition zone thickness of *Lawrence and Shearer* [2006]:

$$\delta z = 242 + \delta T \times \frac{dz}{dP} \times \left[\left(\frac{dP}{dT} \right)_{660} - \left(\frac{dP}{dT} \right)_{410} \right]$$

[21] where δz is the observed transition zone thickness, δT is the temperature anomaly, and $\left(\frac{dP}{dT} \right)_{660}$ and $\left(\frac{dP}{dT} \right)_{410}$ are the Clapeyron slopes for the phase transformations. Assuming values for the Clapeyron slopes of the olivine to wadsleyite and ringwoodite to perovskite phase transitions of 3.1 and -2.6 MPa/K, respectively [*Akogi et al.*, 2007], the δz we observe would suggest that the mantle transition zone beneath Bermuda is ~185 K hotter than the average. The Clapeyron slope of the ringwoodite to perovskite transformation is not well constrained; plausible slopes range between -0.2 and -3.0 MPa/K [*Bina and Helffrich*, 1994; *Ito and Takahashi*, 1989; *Irifune et al.*, 1998; *Katsura et al.*, 2003; *Fei et al.*, 2004; *Litasov et al.*, 2005], yielding a range of possible temperature anomalies between 172 and 320 K for our Bermuda data. Even the lower end of this range suggests a temperature anomaly beneath Bermuda that is similar to seismic estimates of transition zone temperature from other hotspot regions such

as Iceland [*Shen et al.*, 1996] and Ethiopia [*Benoit et al.*, 2006], though ~120–220 K cooler than Hawaii [*Cao et al.*, 2011]. The temperature anomaly is consistent with hotspot temperature anomalies estimated from petrology [e.g., *Herzburg and Gazel*, 2009]. If observed, a weak thermal anomaly relative to other hotspots might explain lack of an age progressive chain and the apparent motion of the source along with the North American plate. However, even the low end of the temperature anomaly we estimate beneath Bermuda is approximately three times larger than that the $\pm$ 50 K predictions from edge-driven convection models by *King and Ritsema* [2000].

[22] Resolving seismic structure beneath oceanic islands is challenging because of the limited horizontal spacing of seismometers. As a result, it may be easier to test the predictions of the edge-driven convection model by imaging the downwelling limbs of edge-driven convection cells than the structure directly beneath an ocean island. This implies that the southeastern US may be the best location to look for evidence for an EDC cell associated with Bermuda. A recent receiver function and shear wave splitting study using permanent broad-band seismic stations in the southeastern US found null shear wave splitting observations (i.e., apparently isotropic mantle) and normal transition zone thickness [*Long et al.*, 2010]. These results are ambiguous, as the radially isotropic mantle is consistent with vertical flow and potentially consistent with EDC, while the normal transition zone thickness is difficult to reconcile with a cold, downwelling limb.

5. Conclusions

[23] Our RF analysis of transition zone discontinuities beneath Bermuda clearly images a thin (215 km) transition zone, approximately 27 km thinner than the global average and consistent with the transition zone thicknesses measured at other hotspots [*Lawrence and Shearer*, 2006]. SKS, SKKS, and PKS arrivals are consistent with apparently isotropic upper mantle beneath Bermuda; this observation represents a perturbation to the WNW-ESE fast anisotropic direction for the western North Atlantic inferred from surface waves [*Lebedev and van der Hilst*, 2008; *Becker et al.*, 2012]. A plausible explanation for the general lack of *KS splitting beneath Bermuda is predominantly vertical mantle flow, resulting in radially isotropic mantle. Taken together, these observations suggest

the presence of hot, buoyant, upwelling mantle beneath Bermuda, with the temperature anomaly possibly extending through the transition zone into the lower mantle.

[24] On the other hand, the depth of the 660 km discontinuity is more consistent with edge-driven convection than a mantle plume origin for Bermuda volcanism. Additionally, there are a host of other independent observations that challenge a simple mantle plume model. These include the lack of present-day volcanic activity, the absence of volcanic activity northeast of Bermuda along the direction of plate motion, and the elongation of the bathymetric swell in a direction oblique to plate motion [*Gripp and Gordon*, 2002] (Figure 1). It is particularly puzzling that we observe a present-day thermal anomaly in the transition zone beneath Bermuda, given that the most recent volcanic activity occurred no later than the early Miocene and the North American plate has moved at least 800 km in a hotspot reference frame since then. This discrepancy poses a major challenge to a model that invokes the North American plate moving over a stationary deep mantle plume. Nevertheless, the observations of radially isotropic upper mantle, a thin transition zone, relatively slow shear velocity anomalies in tomographic models, and the lack of subsidence since the end of volcanic activity would suggest the presence of a buoyant thermal anomaly beneath Bermuda today. If this is indeed due to a mantle plume, the plume must travel with the North American plate. If it is due to edge-driven convection, the magnitude of the thermal anomaly is surprising and the corresponding downwelling limb of the convection cell remains elusive.

Acknowledgment

References

Akaogi, M., H. Takayama, H. Kojitani, H. Kawaji, and T. Atake (2007), Low-temperature heat capacities, entropies and enthalpies of Mg_2SiO_4 polymorphs, and α-β-γ and postspinel phase relations at high pressure, *Phys. Chem. Miner.*, *34*, 169–183, doi:10.1007/s00269-006-0137-3.

Anderson, D. L. (2005), Scoring hotspots: The plume and plate paradigms, in *Plates, Plumes, and Paradigms, Geol. Soc. of Am. Spec. Pap. 388*, GSA, edited by G. R. Foulger et al., pp. 19–29.

Barclay, A. H., and D. R. Toomey (2003), Shear wave splitting and crustal anisotropy at the Mid Atlantic Ridge, 35°N, *J. Geophys. Res.*, *108*(B8), 2378, doi:10.1029/2001JB000918.

Becker, T. W., S. Lebedev, and M. D. Long (2012), On the relationship between azimuthal anisotropy from shear wave splitting and surface wave tomography, *J. Geophys. Res.*, *117*, B01306, doi:10.1029/2011JB008705.

Benoit, M. H., A. A. Nyblade, T. J. Owens, and G. Stuart (2006), Mantle transition zone structure and upper mantle S velocity variations beneath Ethiopia: Evidence for a broad, deep-seated thermal anomaly, *Geochem. Geophys. Geosyst.*, *7*, Q11013, doi:10.1029/2006GC001398.

Bina, C. R., and G. Helffrich (1994), Phase transition Clapeyron slopes and transition zone seismic discontinuity topography, *J. Geophys. Res.*, *99*, 15,853–15,860.

Blackman, D., and J.-M. Kendall (1997), Sensitivity of teleseismic body waves to mineral texture and melt in the mantle beneath a mid-ocean ridge, *Philos. Trans. R. Soc. London A*, *355*, 217–231.

Cao, Q., R. D. van der Hilst, M. V. de Hoop, and S.-H. Shim (2011), Seismic imaging of transition zone discontinuities suggests hot mantle west of Hawaii, *Science*, *332*, 1068–1071, doi:10.1126/science.1202731.

Courtillot, V., A. Davaille, J. Besse, and J. Stock (2003), Three distinct types of hotspots in the Earth's mantle, *Earth Planet. Sci. Lett.*, *205*, 295–308.

Crough, S. T. (1983), Hotspot swells, *Ann. Rev. Earth Planet. Sci.*, *11*, 165–193.

Davies, G. F. (1988), Ocean bathymetry and mantle convection: 1. Large-scale flow and hotspots, *J. Geophys. Res.*, *93*, 10,467–10,480.

Debayle, E., and Y. Ricard (2013), Seismic observations of large-scale deformation at the bottom of fast-moving plates, *Earth Planet. Sci. Lett.*, *376*, 165–177.

Duncan, R. A. (1984), Age progressive volcanism in the New England Seamounts and the opening of the central Atlantic Ocean, *J. Geophys. Res.*, *89*, 9980–9990.

Fei, Y., and C. M. Bertka (1999), Phase transitions in the Earth's mantle and mantle mineralogy, in *Mantle Petrology: Field Observations and High-Pressure Experimentation: A Tribute to F. R. Boyd*, vol. *6*, edited by Y. Fei, C. M. Bertka, and B. O. Mysen, pp. 189-207, Geochemical Society, Houston, TX.

Fei, Y., J. Orman, J. Li, W. Westrenen, C. Sanloup, W. Minarik, K. Hirose, T. Komabayashi, M. Walter, and K. Funakoshi (2004), Experimentally determined postspinel transformation boundary in Mg_2SiO_4 using MgO as an internal pressure standard and its geophysical implications, *J. Geophys. Res.*, *109*, B2305, doi:10.1029/2003JB002562.

Flanagan, M. P., and P. M. Shearer (1998), Global mapping of topography on transition zone velocity discontinuities by stacking SS precursors, *J. Geophys. Res.*, *103*, 2673–2692.

Frassetto, A., G. Zandt, H. Gilbert, T. J. Owens, and C. Jones (2010), Improved imaging with phase-weighted common conversion point stacks of receiver functions, *Geophys. J. Int.*, *182*, 368–374.

Fouch, M. J. and S. Rondenay (2006), Seismic anisotropy beneath stable continental interiors, *Phys. Earth Planet. Inter.*, *158*, 292–320.

Gripp, A. E., and R. G. Gordon (2002), Young tracks of hotspots and current plate velocities, *Geophys. J. Int.*, *150*, 321–364.

Gu, Y. J., A. M. Dziewonski, and C. B. Agee (1998), Global de-correlation of the topography of transition zone discontinuities, *Earth Planet. Sci. Lett.*, *157*, 57–67.

Helffrich, G. (2000), Topography of the transition zone seismic discontinuities, *Rev. Geophys.*, *38*, 141–158.

Herzburg, C., and E. Gazel (2009), Petrologic evidence for secular cooling in mantle plumes, *Nature*, *458*(7238), 619–622.

Houser, C., G. Masters, P. Shearer, and G. Laske (2008), Shear and compressional velocity models of the mantle from cluster analysis of long-period waveforms, *Geophys. J. Int.*, *174*, 195–212.

Irifune, T., et al. (1998), The postspinel phase boundary in Mg_2SiO_4 determined by in situ X-ray diffraction, *Science*, *279*, 1698–1700.

Ito, E., and E. Takahashi (1989), Post-spinel transformation in the system $MgSiO_3$–Fe_2SiO_4 and some geophysical implications, *J. Geophys. Res.*, *94*, 10,637–10,646.

Jackson, I. (1983), Some geophysical constraints on the chemical composition of the earth's lower mantle, *Earth Planet. Sci. Lett.*, *62*, 91–103.

Juliá, J., and A. A. Nyblade (2013), Probing the upper mantle transition zone under Africa with P520s conversions: Implications for temperature and composition, *Earth Planet. Sci. Lett.*, *368*, 151–162.

Katsura, T., and E. Ito (1989), The system Mg_2SiO_4 – Fe_2SiO_4 at high pressures and temperatures: Precise determination of stabilities of olivine, modified spinel, and spinel, *J. Geophys. Res.*, *94*, 15,663–15,670.

Katsura, T., et al. (2003), Post-spinel transition in Mg_2SiO_4 determined by high P–T in situ X-ray diffractometry, *Phys. Earth Planet. Int.*, *136*, 11–24.

Kennett, B. L. N., E. R. Engdahl, and R. Buland (1995), Constraints on seismic velocities in the earth from travel times, *Geophys. J. Int.*, *122*, 108–124.

Kind, R., and L. P. Vinnik (1988), The upper mantle discontinuities underneath the GRF array from P-to-S converted phases, *Geophys. J.*, *62*, 138–147.

King, S. D. (2007), Hotspots and edge-driven convection, *Geology*, *35*, 223–226.

King, S. D., and D. L. Anderson (1998), Edge driven convection, *Earth Planet. Sci. Lett.*, *160*, 289–296.

King, S. D., and J. Ritsema (2000), African hotspot volcanism: Small-scale convection in the upper mantle beneath cratons, *Science*, *290*, 1137–1140.

Kustowski, B., G. Ekström, and A. M. Dziewonski (2008), Anisotropic shear-wave velocity structure of the Earth's mantle: A global model, *J. Geophys. Res.*, *113*, B06306, doi:10.1029/2007JB005169.

Lawrence, J. F., and P. M. Shearer (2006), A global study of transition zone thickness using receiver functions, *J. Geophys. Res.*, *111*, B06307, doi:10.1029/2005JB003973.

Leahy, G. M., and D. Bercovici (2007), On the dynamics of a hydrous melt layer above the transition zone, *J. Geophys. Res.*, *112*, B07401, doi:10.1029/2006JB004631.

Lebedev, S., and R. D. van der Hilst (2008), Global upper-mantle tomography with the automated multimode inversion of surface and S-waveforms, *Geophys. J. Int.*, *173*, 505–518.

Ligorría, J. P., and C. J. Ammon (1999), Iterative deconvolution and receiver function estimation, *Bull. Seismol. Soc. Am.*, *89*, 1395–1400.

Litasov, K., E. Ohtani, A. Sano, A. Suzuki, and K. Funakoshi (2005), In situ X-ray diffraction study of post-spinel transformation in a peridotite mantle: Implication for the 660-km discontinuity, *Earth Planet. Sci. Lett.*, *238*, 311–328.

Lizarralde, D., J. B. Gaherty, J. A. Collins, G. Hirth, and S. Kim (2004), Spreading-rate dependence of melt extraction at mid-ocean ridges from mantle seismic refraction data, *Nature*, *432*, 744–747.

Long, M. D. (2013), Constraints on subduction geodynamics from seismic anisotropy, *Rev. Geophys.*, *51*, 76–112, doi:10.1002/rog.20008.

Long, M. D., M. H. Benoit, M. C. Chapman, and S. D. King (2010), Upper mantle anisotropy and transition zone thickness beneath southeastern North America and implications for mantle dynamics, *Geochem. Geophys. Geosyst.*, *11*, Q10012, doi:10.1029/2010GC003247.

Lynner, C., and M. D. Long (2012), Evaluating contributions to SK(K)S splitting from lower mantle anisotropy: A case study from station DBIC, Cote D'Ivoire, *Bull. Seismol. Soc. Am.*, *102*, 1030–1040.

Morgan, W. J. (1983), Hotspot tracks and the early rifting of the Atlantic, *Tectonophysics*, *94*, 123–139.

Morgan, W. J., and S. T. Crough (1979), Bermuda hotspot and the Cape Fear Arch, *Eos Trans. AGU*, *60*, 392–393.

Mueller, R. D., J-Y. Royer, and L. A. Lawver (1993), Revised plate motions relative to hotspots from combined Atlantic and Indian Ocean hotspot tracks, *Geology*, *21*, 275–278.

Panning, M., and B. Romanowicz (2006), A three dimensional radially anisotropic model of shear velocity in the whole mantle, *Geophys. J. Int.*, *167*, 361–379, doi:10.1111/j.1365-246X.2006.03100.x.

Ringwood, A. E. (1983), *Composition and petrology of the earth's mantle*, McGraw-Hill, New York.

Ritsema, J., A. Deuss, H. J. van Heijst, and J. H. Woodhouse (2010), S40RTS: A degree-40 shear-velocity model for the mantle from new Rayleigh wave dispersion, teleseismic traveltime and normal-mode splitting function measurements, *Geophys. J. Int.*, *184*(3), 1223–1236, doi:10.1111/j.1365-246X.2010.04884.x.

Saikia, A., D. J. Frost, and C. Rubie (2008), Splitting of the 520-kilometer seismic discontinuity and chemical heterogeneity in the mantle, *Science*, *319*, 1515–1518.

Schimmel, M., and H. Paulssen (1997), Noise reduction and detection of weak, coherent signals through phase-weighted stacks, *Geophys. J. Int.*, *130*(2), 497–505.

Shearer, P. M. (1990), Seismic imaging of upper-mantle structure with new evidence for a 520-km discontinuity, *Nature*, *344*, 121–126.

Shen, Y., S. C. Solomon, I. Th. Bjarnason, and G. M. Purdy (1996), Hot mantle transition zone beneath Iceland and the adjacent Mid-Atlantic Ridge inferred from *P*-to-*S* conversions at the 410- and 660-km discontinuities, *Geophys. Res. Lett.*, *23*, 3527-3530.

Simmons, N. A., A. M. Forte, and S. P. Grand (2009), Joint seismic, geodynamic and mineral physical constraints on three-dimensional mantle heterogeneity: Implications for the relative importance of thermal versus compositional heterogeneity, *Geophys. J. Int.*, *177*, 1284–1304.

Sleep, N. H. (1990), Hotspots and mantle plumes: Some phenomenology, *J. Geophys. Res.*, *95*, 6715–6736.

Sleep, N. H. (2002), Ridge-crossing mantle plumes and gaps in tracks, *Geochem. Geophys. Geosyst.*, *3*(12), 8505, doi:10.1029/200GC000290.

Smyth, J. R., D. J. Frost, F. Nestola, C. M. Holl, and G. Bromiley (2006), Olivine hydration in the deep upper mantle: Effects of temperature and silica activity, *Geophys. Res. Lett.*, *33*, L15301.

Smyth, J. R., and S. D. Jacobsen (2006), Nominally anhydrous minerals and Earth's deep water cycle, edited by S. D. Jacobsen, and S. van der Lee, pp. 1–11, Am. Geophys. Union, Washington, DC.

The Shipboard Scientific Party (1979), Site 386: Fracture valley sedimentation on the central Bermuda Rise, in *Initial*

Reports of the Deep Sea Drilling Project, vol. *43*, edited by B. E. Tucholke and P. R. Vogt, pp. 195–321, U.S. Gov. Print. Off., Washington, D. C.

Tucholke, B. E., and P. R. Vogt (1979), Western North Atlantic: Sedimentary evolution and aspects of tectonic history, in *Initial Reports of the Deep Sea Drilling Project*, vol. *43*, edited by B. E. Tucholke and P. R. Vogt, pp. 791–825, U.S. Gov. Print. Off., Washington, D. C.

Van der Lee, S. K., and D. A. Wiens (2006), Seismological constraints on Earth's deep water cycle, in *Earth's Deep Water Cycle*, edited by S. D. Jacobsen, and S. van der Lee, pp. 13–27, Am. Geophys. Union, Washington, DC.

Vogt, P. R., and W.-Y. Jung (2007), Origin of the Bermuda volcanoes and the Bermuda Rise: History, observations, models, and puzzles, in *Plates, Plumes, and Planetary Processes, Geol. Soc. Am. Spec. Pap. 430*, GSA, edited by G. R. Foulger and D. M. Jurdy, pp. 553–591:, doi10.1130/2007.2430(27).

Wang, Y., D. J. Weidner, R. C. Liebermann, and Y. Zhao (1994), P-V-T equation of state of (Mg, Fe)SiO$_3$ perovskite: Constraints on composition of the lower mantle, *Phys. Earth Planet. Inter.*, *83*, 13–40.

Wüstefeld, A., G. Bokelmann, G. Barruol, and C. Zaroli (2007), SplitLab: A shear-wave splitting environment in MATLAB, *Comp. Geosci.*, *34*, 515–528.